Electrochemical – chemical cycle for high-efficiency decoupled water splitting in a near-neutral electrolyte

Ilya Slobodkin,[1,§] Elena Davydova,[1, §] Matan Sananis,[1] Anna Breytus[1] and Avner Rothschild[1,2*]

[1] Department of Materials Science and Engineering, Technion – Israel Institute of Technology, Haifa, Israel

[2] The Nancy & Stephen Grand Technion Energy Program (GTEP), Technion – Israel Institute of Technology, Haifa, Israel

[§] These authors contributed equally to this work

* E-mail: avnerrot@technion.ac.il

Abstract

Green hydrogen produced by water splitting using renewable electricity is essential to achieve net-zero carbon emissions. Present water electrolysis technologies are uncompetitive with low-cost grey hydrogen produced from fossil fuels, limiting their scale-up potential. Disruptive processes that decouple the hydrogen and oxygen evolution reactions and produce them in separate cells or different stages emerge as a prospective route to reduce system cost by enabling operation without expensive membranes and sealing components. Some of them divide the hydrogen or oxygen evolution reactions into electrochemical and chemical sub-reactions, leading the way to high efficiency. However, high efficiency was demonstrated only in a batch process with thermal swings that present operational challenges. This work introduces a breakthrough process that produces hydrogen and oxygen in separate cells and supports high-efficiency continuous operation in a membraneless system. We demonstrate high Faradaic and electrolytic efficiency and high-rate operation in a near-neutral electrolyte of NaBr in water.

Introduction

Green hydrogen produced by water splitting using renewable energies such as solar and wind is essential to reduce greenhouse gas emissions, especially in hard-to-abate industrial sectors such as steel, cement and ammonia production. At present, water electrolysis technologies are unable to compete with the low cost of grey hydrogen production by steam methane reforming (SMR),[1] an industrial process that provides most of the hydrogen we use today and produces greenhouse gases (CO_2 and methane) about twenty times more than the amount of hydrogen produced.[2] Therefore, there is a pressing need to improve water electrolysis so as to support low-cost production of green hydrogen at terawatt scale. Towards this aim, decoupled water electrolysis (DWE) where the hydrogen and oxygen evolution reactions (HER and OER, respectively) are decoupled in time and/or place presents a disruptive concept that has spurred innovative efforts to develop membraneless water electrolysis over the past decade.[3,4,5] DWE may lead the way to safe operation without membranes,[6,7,8,9] providing new opportunities to reshape water electrolysis and potentially overcome the fundamental barriers of this century-old technology.

DWE was first reported by Symes and Cronin in 2013, introducing phosphomolybdic acid as a soluble redox couple (SRC) that functions as an electron-coupled-proton buffer (ECPB) and mediates the electron-coupled-proton exchange between the anodic OER and cathodic HER.[10] To function as an effective mediator, the SRC must have a redox potential between the HER and OER potentials. Despite generating oxygen and hydrogen at different times in stepwise stages, a membrane was used to prevent redox shuttling of the polyoxomolybdate anions between the electrodes, and the efficiency was lower than conventional water electrolysis. Low efficiency is an inherent disadvantage of this method since the oxidation and reduction overpotentials of the SRC add up to those of the OER and HER, thus necessitating a larger voltage than in conventional water electrolysis without redox mediators.[5] Subsequent studies pursuing this approach introduced different ECPBs in acidic electrolytes, but the efficiency remained low and a membrane was still necessary.[11,12,13] Another disadvantage of these systems is the use of platinum group metal (PGM) catalysts, which is necessary due to operation in acid electrolytes. To address this limitation, Li et al. introduced alternative SRCs that function as proton-independent electron reservoirs and demonstrated DWE in a wide pH range from neutral to alkaline electrolytes.[14] Without a proton buffer, substantial changes in pH were observed during operation resulting in low efficiency.

Another DWE scheme was reported by Chen et al.[6] and by Landman et al.,[7] replacing the SRC by solid redox electrodes (SRE) that mediate the hydroxide ion (OH^-) exchange between the primary electrodes (cathode and anode) in alkaline electrolyte. To this end, nickel (oxy)hydroxide electrodes such as those commonly used in rechargeable alkaline batteries were employed as auxiliary electrodes that mediate the hydroxide ion exchange between the HER at the cathode of one cell and the OER at the anode of another cell. Thereby, the electrolytic cell was divided into two separate cells that generate hydrogen and oxygen remotely from each other. This enables operation without membranes, paving the way for membraneless DWE. However, using stationary SRE requires batch operation to regenerate the auxiliary electrodes (e.g., by swapping them from one cell to another) when they are fully (dis)charged, whereas SRCs support continuous operation in a flow system much like conventional electrolyzers.[15] Although the reported DWE systems with SRE are less efficient than state-of-the-art alkaline electrolyzes, for the same reason as described above for the case of SRC, they might serve unique purposes such as centralized hydrogen production in photoelectrochemical water splitting. [6,16] Another merit of this approach is operation in alkaline electrolytes, thereby supporting the use of nickel-based catalysts instead of PGM catalysts in acidic electrolytes.

A different DWE approach was reported by Rausch et al., introducing an electrochemical – chemical cycle (ECC) whereby silicotungstic acid was applied as an SRC that was reduced electrochemically at the cathode while oxygen evolved at the anode, and then transferred into another cell where it was oxidized chemically and released hydrogen upon contact with a platinum catalyst (without applying electricity).[17,18] The electrolytic efficiency was 63%$_{HHV}$, and a membrane divided the electrolytic cell to prevent redox shuttling between the electrodes. The next leap in the evolution of DWE was reported by Dotan et al., introducing an electrochemical – thermally-activated chemical (E-TAC) cycle that divides the OER into two sub-reactions and enables operation in near thermoneutral conditions.[8] In the first stage (E), a cobalt-doped nickel hydroxide anode was electrochemically charged to nickel oxyhydroxide while hydrogen evolved at the cathode. This stage was performed in a cold (~25°C) alkaline electrolyte, and it was stopped prior to the onset of oxygen evolution. Then, in the second stage (TAC), the cold electrolyte was replaced by a hot one (95°C) that induced fast spontaneous reaction between the charged anode and water, regenerating the anode back to its initial state while producing oxygen, thereby completing the water decomposition cycle. The E-TAC process presents important advantages: membraneless operation with a remarkable electrolytic efficiency of 98.7%$_{HHV}$ (at the cell level) at a current density of 50 mA/cm^2,[8] identifying it as a potential competitor to conventional water electrolysis.[19,20]

However, the E-TAC process also presents challenges that emerge from batch operation with frequent thermal swings between the E and TAC stages, as well as from capacity and rate limitations of the nickel (oxy)hydroxide anodes, similarly to other battery electrodes.[21] These limitations can be circumvented altogether by shifting the charge storage from the solid nickel (oxy)hydroxide anode to the liquid electrolyte, thereby enabling continuous instead of batch operation and avoiding kinetic limitations that arise from solid state diffusion and phase transformations.[22] This work presents a proof-of-concept of this new approach, using a SRC that stores and releases oxygen instead of hydrogen[17] and demonstrates membraneless DWE in a continuous and isothermal process (without thermal swings) with high efficiency and high current density.

Concept

We propose an electrochemical – chemical cycle that divides the OER into two sub-reactions, electrochemical and chemical ones, similarly to the E-TAC cycle.[8] But instead of using an SRE such as the nickel (oxy)hydroxide anode in E-TAC, we propose an SRC that supports continuous operation in an isothermal process with high efficiency and high rate. Furthermore, our process operates in a near-neutral salt electrolyte instead of the strong acid used in previous reports on DWE with SRC.[10-13,17] The key to achieving these merits is an SRC that its reduced state (*red*) is oxidized in an electrochemical reaction ($red \rightarrow ox + ne^-$) that complements the HER without evolving oxygen or other volatile side products, and, in the presence of suitable catalyst, its oxidized state (*ox*) evolves oxygen spontaneously in a chemical reaction that reduces it back to its reduced state ($ox \rightarrow red + O_2$). To provide a driving force for this chemical reaction, the SRC should have a reversible redox potential (E^0) above the thermodynamic OER potential (1.23 V_{RHE}), whereas for high efficiency it should be oxidized at a low overpotential, and ideally below the OER onset potential (~1.6 V_{RHE} for state-of-the-art OER catalysts).[23] This dictates an SRC with a reversible redox potential of ~1.4 V_{RHE}, similar to that of the nickel (oxy)hydroxide electrodes used in the E-TAC process.[8] We note that our process modifies the OER whereas the one reported by Rausch et al. modifies the HER.[17] This salient difference is the key to achieving high efficiency in our process, as demonstrated below. Based on these criteria, the bromide (Br^-) / bromate (BrO_3^-) couple (E^0 = 1.42 V_{RHE})[24] was selected as the SRC for our process (**Figure 1**). The salts of both the reduced and oxidized species, NaBr and $NaBrO_3$, have high solubility in water, 946 and 394 g/L, respectively (at 25°C).[25] Moreover, the bromine (Br_2) produced at the anode is denser

than water (3.1 g/cm^3)[25] and is highly soluble in water (34 g/L at 25 °C),[26] which minimizes the risk of evaporation and entrainment by the hydrogen bubbles produced at the cathode. This makes the Br^-/BrO_3^- couple preferable over the Cl^-/ClO_3^- couple that produces volatile chlorine (Cl_2) with low solubility in water (6.3 mg/L at 25°C)[27] which results is a Faradaic loss.[28]

Figure 1 illustrates our DWE process for the decoupled production of hydrogen and oxygen in separate cells, using Br^-/BrO_3^- as an SRC that stores and releases oxygen by turns. The system comprises separated electrolytic and catalytic cells that produce hydrogen and oxygen, respectively. The two cells are connected to each other by a joint electrolyte flow. The electrolytic cell comprises two electrodes, a cathode that generates hydrogen by the HER (rxn 1), and an anode where the bromide electrooxidation reaction (BER, rxn 2) takes place:

$$2H^+ + 2e^- \rightarrow H_2 \quad (1)$$
$$2Br^- \rightarrow Br_2 + 2e^- \quad (2)$$

According to studies on bromide electrolysis,[29,30] the bromine molecules (Br_2) produced at the anode react with water in the bulk of the aqueous electrolyte to form hypobromous acid (HBrO, rxn 3) that forms hypobromite anions (BrO^-) and protons by dissociation (rxn 4). The hypobromite anions react with hypobromous acid to form bromate anions (BrO_3^-, rxn 5), the desired product:

$$Br_2 + H_2O \rightleftharpoons HBrO + H^+ + Br^- \quad (3)$$
$$HBrO \rightleftharpoons H^+ + BrO^- \quad (4)$$
$$2HBrO + BrO^- \rightarrow BrO_3^- + 2Br^- + 2H^+ \quad (5)$$

The overall anode-related process, rxns 2 – 5, can be summarized by rxn 6:

$$Br^- + 3H_2O \rightarrow BrO_3^- + 6H^+ + 6e^- \quad (6)$$

resulting in an $e^-/H_2/BrO_3^-$ ratio of 6/3/1. For brevity, **Figure 1** illustrates the anodic-related reactions (rxns 2 – 5) as one (rxn 6).

The HBrO and BrO^- intermediate products may lead to undesired side reactions:[30]

$$6BrO^- + 3H_2O \rightarrow 2BrO_3^- + 6H^+ + 4Br^- + 1.5O_2 + 6e^- \quad (7)$$
$$HBrO + 2e^- \rightarrow Br^- + OH^- \quad (8)$$
$$BrO^- + H_2O + 2e^- \rightarrow Br^- + 2OH^- \quad (9)$$
$$BrO_3^- + 3H_2O + 6e^- \rightarrow Br^- + 6OH^- \quad (10)$$
$$BrO_3^- + 2H_2O + 4e^- \rightarrow BrO^- + 4OH^- \quad (11)$$

To suppress rxn 7, the electrolyte temperature and pH must be tuned to reach an optimal degree of HBrO dissociation (rxn 4) that gives rise to an optimal ratio between the intermediate products that lead to high selectivity for the production of bromate (BrO_3^-). Operation at 60°C and pH 8 was found to provide optimal conditions to suppress oxygen evolution (rxn 7) and achieve close to 100% Faradic efficiency for bromate production (rxn 6).[31,32] To suppress the cathodic backward reactions that reduce the oxidized bromine species back to bromide (rxns 8 – 11), a small amount (1–3 g/L) of sodium dichromate ($Na_2Cr_2O_7$) is added to the sodium bromide (NaBr) aqueous electrolyte. The dichromate anions ($Cr_2O_7^{2-}$) are reduced and deposited on the cathode, coating it with a semipermeable chromium hydroxide layer (illustrated by the green layer in **Figure 1**) that suppresses the cathodic loss reactions (rxns 8 – 11), while allowing the HER to occur without hindrance. This is also done in chloride electrolysis for the same reason.[33] Adding $Na_2Cr_2O_7$ enables to achieve high Faradaic efficiency without needing a membrane to divide the cell into anodic and cathodic compartments, supporting our aim to develop a membraneless process.

The catalytic cell consists of a column embedded with a catalyst (**Figure 1**, right) that facilitates the catalytic decomposition of bromate (BrO_3^-) anions formed in the electrolytic cell into bromide (Br^-) and oxygen (O_2), thereby regenerating the electrolyte and evolving oxygen:

$$2BrO_3^- \rightarrow 2Br^- + 3O_2 \qquad (12)$$

The electrolytic and catalytic cells are connected into a flow system that provides continuous electrolyte flow from one cell to another, taking the oxidized bromate-rich electrolyte from the bottom of the electrolytic cell to the bottom of the catalytic cell. The catalytic cell regenerates the electrolyte to its bromide-rich reduced state, and the reduced electrolyte flows from the top of the catalytic cell back to the top of the electrolytic cell, as illustrated in **Figure 1**.

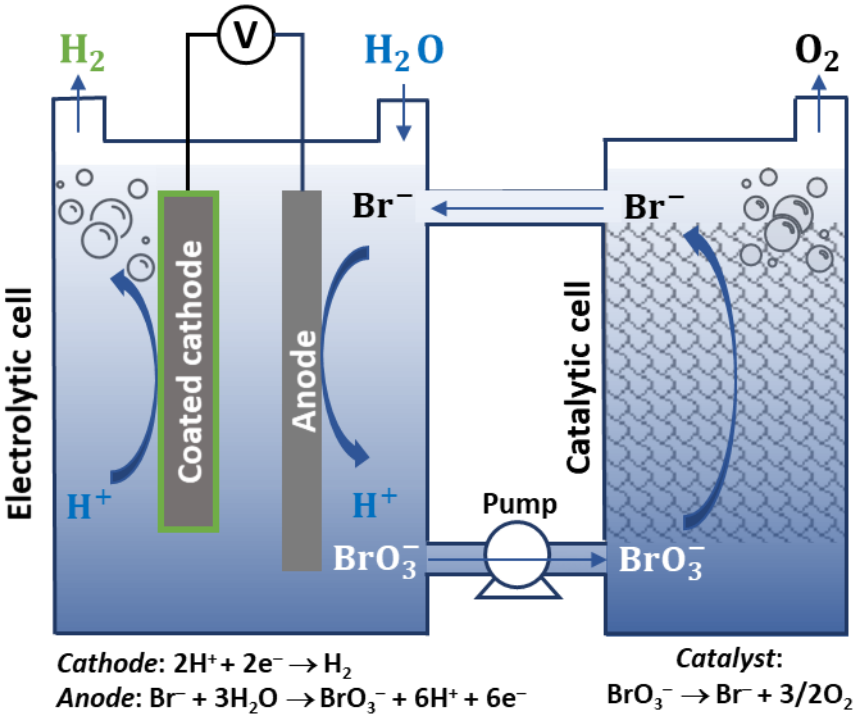

Figure 1: Schematic illustration of the proposed DWE process with continuous generation of H_2 and O_2 in separate electrolytic and catalytic cells using Br^-/BrO_3^- as a soluble redox couple.

Proof-of-concept

The feasibility of the proposed DWE process (**Figure 1**) was validated separately in two sets of experiments that examine the performance of the electrolytic and catalytic sub-processes. Then, complementary measurements were carried out combining the two sub-processes into a unified batch-to-bath process that splits water into hydrogen and oxygen in separate cells.

Electrolytic process: The electrolytic process was examined in two operational modes. The first (main) mode corresponds to bromate electrolysis in 1.5M NaBr electrolyte with the addition of 3.8 mM $Na_2Cr_2O_7$, where the electrolyte was heated to 60°C and stirred during the process. In the second mode, we examined the possibility to carry out the process in a pristine 1.5M NaBr electrolyte without the toxic $Na_2Cr_2O_7$ additive by utilizing the phase separation between the high-density bromine (Br_2) that forms on the anode (rxn 2) and the rest of the electrolyte to minimize the diffusion of reaction products to the cathode and suppress cathodic loss reactions (rxns 8 – 11). To suppress mixing the heavier and lighter parts of the electrolyte, the electrolysis was carried out in an unheated electrolyte

(~20°C) without stirring. **Figure 2** presents photographs of the electrolysis tests carried out in the first mode (**Figures 2a-b**) and in the second mode (**Figures 2c-d**). In both cases, the anode (RuO_2-TiO_2/Ti DSA) and cathode (Pt foil in the first mode and Pt coil is the second mode) were placed in an electrolytic cell with no membrane or diaphragm division. The addition of $Na_2Cr_2O_7$ in the first operational mode resulted in a yellowish solution (prior to electrolysis), as shown in **Figure 2a**, whereas in its absence in the second mode the electrolyte was colorless (**Figure 2c**). During operation in the first mode (**Figure 2b**), the whole volume of the electrolyte becomes cloudy due to the evolution of hydrogen bubbles that were stirred throughout the cell. The electrolyte color remained yellowish, comprising contributions from both the $Cr_2O_7^{2-}$ anions and the bromide oxidation intermediates. The operation in the second mode resulted in an intense hydrogen bubbles formation at the top of the cell, along with a phase separation between the red Br_2-rich oxidized solution that sank down to the bottom of the cell, and the yellowish solution that contained some small amount of oxidized bromine species in the upper part of the cell (**Video S1**). Post-electrolysis stirring turned the phase-separated red and yellowish solutions into a homogeneous yellowish solution (**Figures 2, e1-e5** and **Video S2**), indicating that the Br_2-rich solution reacted with the rest of the electrolyte according to rxns 3 – 5. However, a residual amount of unreacted intermediate products remained, as indicated by the yellow color of the stirred solution.

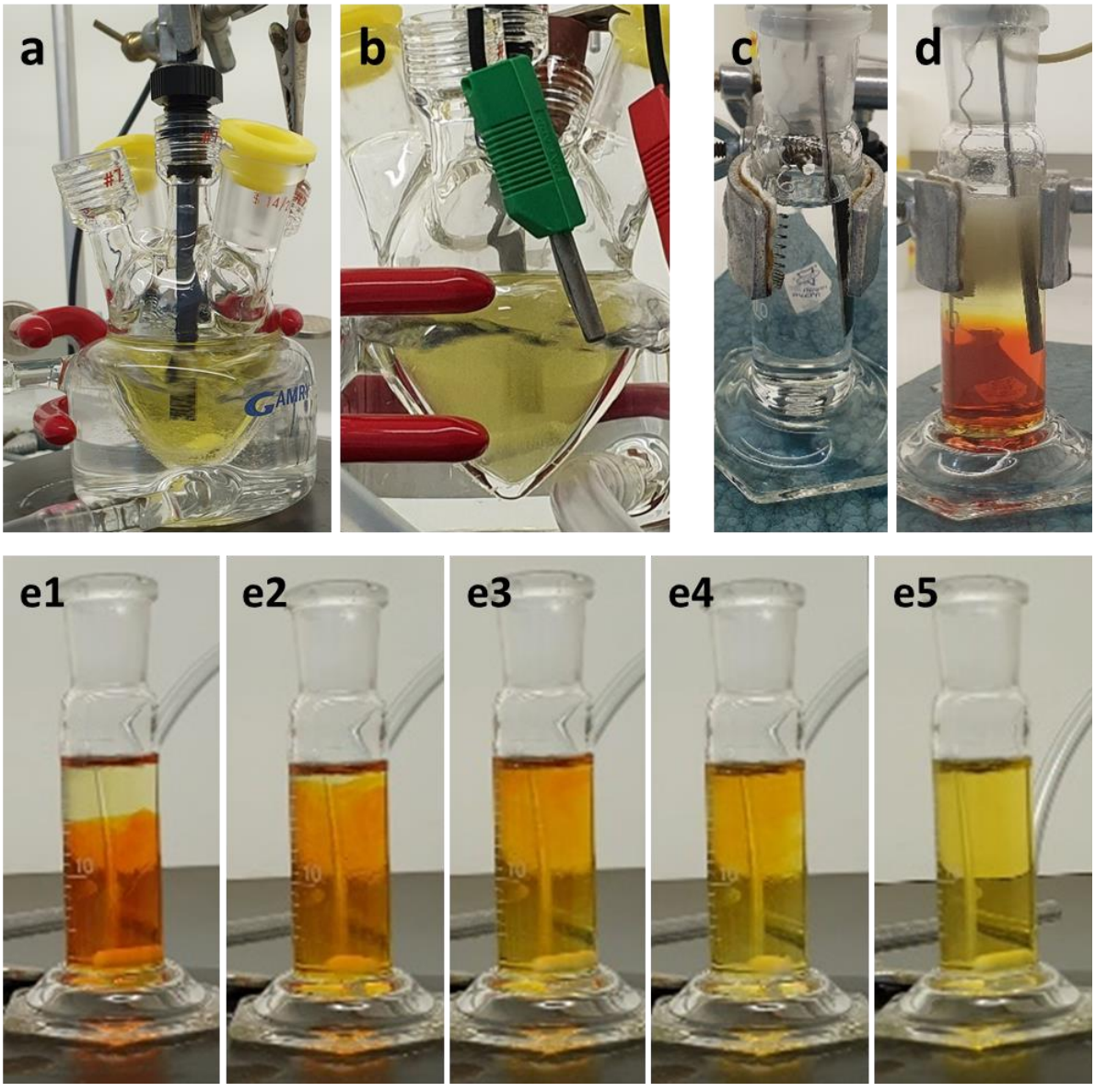

Figure 2. Bromide electrolysis tests. Photographs of the electrolytic cells we used to examine the bromide electrolysis process with stirred **(a-b)** and still **(c-e)** electrolytes. **(a)** and **(c)** before electrolysis; **(b)** and **(d)** during electrolysis; **(e1-e5)** sequential snapshots during subsequent stirring after electrolysis (see **Video S2**). The electrolyte composition and other experimental conditions are specified in the **Methods** section and are summarized in **Extended Data Table 1**.

The Faradaic efficiency of bromide electrooxidation was examined for both operational modes, with and without $Na_2Cr_2O_7$, by electrolyzing 20 ml of 1.5M NaBr electrolyte (without buffers) for 5.36 hours at a current of 600 mA (total charge 11578 C) and analyzing the resulting bromate content by iodometric titration (**Video S3**). Considering that six electrons are needed to oxidize a bromide anion to a bromate anion (rxn 6), this charge should produce 0.02 moles of bromate anions at 100% Faradaic efficiency and convert 2/3 (1M) of the bromide anions in the initial electrolyte (20 ml of 1.5M NaBr) to bromate anions. In the first operational mode (**Figure 2b**), with the $Na_2Cr_2O_7$ additive and stirring, the Faradaic efficiency was 98±2%, indicating that these operation conditions suppress both the cathodic side reactions (rxns 8 -11) as well as the anodic OER (rxn 7). A direct confirmation of no OER interference is presented in **Video S4**, showing bromide electrolysis in a Hoffman apparatus with no oxygen evolution. Without the $Na_2Cr_2O_7$ additive (but otherwise the same conditions), the Faradaic efficiency dropped to 10±1%, indicating the important role of $Na_2Cr_2O_7$ to prevent rxns 8 – 11 by forming a polyoxide cathodic barrier, as reported elsewhere.[29,31,32,33,34,35,36]

In the second operational mode (**Figure 2d**), without $Na_2Cr_2O_7$, the Faradaic efficiency was 72±2% without stirring, and it dropped to 13±1% with stirring, demonstrating the effectiveness of the spontaneous phase separation between the oxidized electrolyte and the rest of the electrolyte in suppressing the cathodic loss reactions (rxns 8 – 11). This encouraging result suggests that the Faradaic efficiency may be further enhanced by removing the oxidized electrolyte from the bottom of the cell, as illustrated in **Figure 1**. This approach may lead the way to high efficiency operation in a benign NaBr electrolyte without $Na_2Cr_2O_7$. A similar approach has been reported in membraneless zinc-bromine redox flow batteries, harnessing the phase separation in the electrolyte to suppress backward reactions like those occurring in our system.[37] An alternative solution to suppress the cathodic loss reactions without using $Na_2Cr_2O_7$ is precoating the cathode (*ex-situ*) with a chromium polyoxide (or other) layer instead of *in-situ* deposition of $Cr_2O_7^{2-}$ anions during operation in the presence of $Na_2Cr_2O_7$. We have achieved partial success pursuing this approach by using a precoated cathode that was taken after going through previous electrolysis tests with $Na_2Cr_2O_7$ in the solution, reaching a Faradaic efficiency of 80±2% in subsequent tests without $Na_2Cr_2O_7$. We suspect that the lower Faradaic efficiency of the precoated cathode with respect to *in-situ* coating during electrolysis in the presence of $Na_2Cr_2O_7$ in the electrolyte may arise detachment of small segments of the coating layer during operation. In the presence of $Cr_2O_7^{2-}$ anions in the electrolyte the barrier layer is more effective than the *ex-situ* precoating, probably due to self-healing of the polyoxide layer during operation. Long-term tests demonstrate the process stability, in the presence of $Na_2Cr_2O_7$, during continuous operation over 5 days (120 h), as shown in **Extended Data Figure 1.**

Further to the Faradaic efficiency measurements, the electrolytic (i.e., voltage) efficiency was measured for the first operational mode (**Figure 2b**) that demonstrated the highest Faradaic efficiency (98±2%). This was done by two-electrode galvanostatic voltammetry measurements at different current densities ranging from 5 to 1000 mA/cm^2 (**Extended Data Figure 2**). **Figure 3a** presents the steady state current density vs. voltage (IR-corrected) results obtained for bromide electrolysis in unbuffered (black) and buffered (0.7M borate buffer, blue) 1.5M NaBr electrolytes with 3.8 mM $Na_2Cr_2O_7$, heated to 60°C and stirred at 400 rpm. Introducing 0.7M borate buffer decreases the cell voltage by ~0.2 V at current densities up to 50 mA/cm^2, resulting in a low onset voltage of 1.5 V at 5

mA/cm^2. The reduction in cell voltage remains significant even at 200 mA/cm^2. A cell voltage of 2.4 V was obtained at a high current density of 1 A/cm^2. Consequently, the electrolytic cell efficiency increased from 86 to 97%$_{HHV}$ at 5 mA/cm^2, and from 75 to 85%$_{HHV}$ at 50 mA/cm^2 (**Figure S1**). Comparing our results (black and blue curves) with previous reports on DWE, marked by red symbols (◊, ♦ and *), shows that the electrolytic performance of our process surpasses previous DWE reports using SRC and SRE (marked by open and solid squares, ◊ and ♦, respectively), except for the E-TAC process (marked by stars, *). E-TAC water electrolysis presents the lowest cell voltage, 1.5 V at a current density of 50 mA/cm^2,[8] but it only goes as high as 100 mA/cm^2 whereas our process reaches 1 A/cm^2. It is also noted that, unlike E-TAC which is a batch process with frequent thermal swings that require additional thermal energy to heat the hot electrolyte at the transition from the cold stage to the hot stage,[8] our process is designed to operate under continuous and isothermal electrolyte flow (**Figure 1**), avoiding this thermal loss. As a result, the gap between the efficiency at the cell level and system level, which can only be examined in a scaled-up system, is expected to be smaller for our process. We also note that stable operation was observed on extended galvanostatic measurements for 5.5 h (**Extended Data Figure 3**).

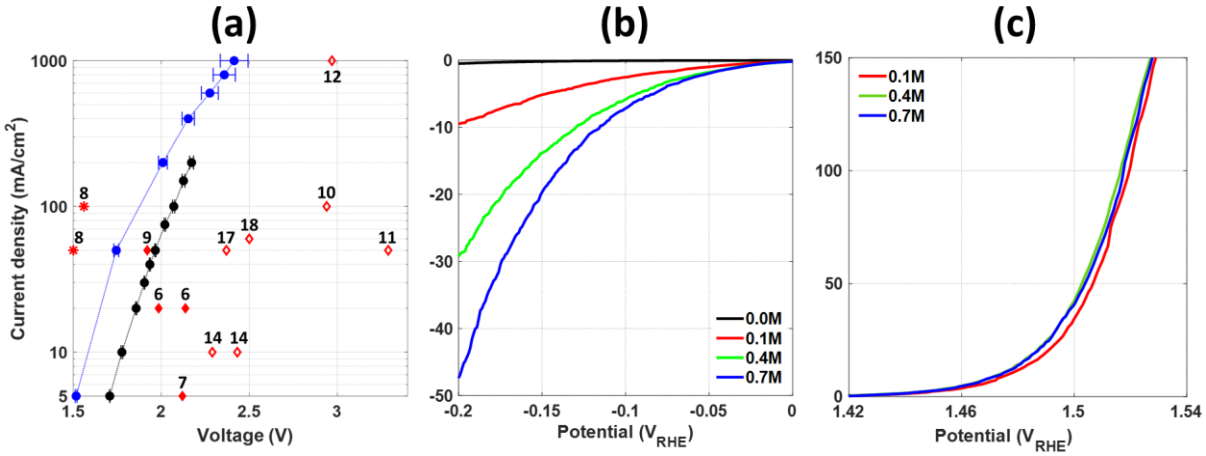

Figure 3. Electrolytic efficiency of bromide electrolysis. (a) Steady state current density vs. voltage (IR-corrected) results (**Table S1**) obtained by galvanostatic measurements at different current densities (**Extended Data Figure 2**) during bromide electrolysis with (blue curve) and without (black curve) borate buffer (0.7M). For comparison, results from previous DWE reports are marked by red symbols (◊ for SRC, ♦ for SRE, and * for E-TAC) and labeled by the respective references. The electrolyte composition at the beginning of the electrolysis measurements was 1.5M NaBr plus 3.8 mM $Na_2Cr_2O_7$, with and without borate buffer (0.7M). The electrolyte was heated to 60°C and stirred at 400 rpm. **(b)** and **(c)** Current density vs. potential (IR-corrected) curves of the Pt foil cathode and RuO_2-TiO_2/Ti DSA anode, respectively, obtained by linear sweep voltammetry (LSV) measurements with a potential scan rate of 1 mV/s. The experimental conditions are specified in the **Methods** section and are summarized in **Extended Data Table 2**.

To assess the individual contributions of the cathodic and anodic reactions to the voltage of our process, we analyzed the cathodic (HER) and anodic (BER) polarization losses by means of LSV measurements in a three-electrode cell. The results are presented in **Figures 3b** and **3c**, showing the current density as a function of the potential of the Pt foil cathode and RuO_2-TiO_2/Ti DSA anode, respectively. The LSV measurements were carried out in 1.5M NaBr electrolytes containing different borate buffer concentrations (0, 0.1, 0.4 and 0.7 M, marked by black, red, green, and blue curves, respectively), under the same conditions (60°C, pH 8) as in the first operational mode of the galvanostatic voltammetry measurements except for not adding $Na_2Cr_2O_7$. One can see that the

cathodic reaction (**Figure 3b**) requires a much higher overpotential than the anodic counterpart (**Figure 3c**), e.g., above 0.2 V at a cathodic current density of 50 mA/cm^2 as compared to less than 0.1 V at the same anodic current density. Thus, the HER presents the main polarization loss in our electrolytic process. The addition of borate buffer enhances the HER kinetics and reduces the cathodic overpotential loss substantially (**Figure 3b**), with negligible effect on the anodic loss (**Figure 3c**). The beneficial effect of the borate buffer in reducing the cathodic overpotential loss is attributed to serving as a proton source in our near neutral NaBr electrolyte[38] and suppressing local pH gradient at the cathode.[39]

Catalytic process: The kinetics of bromate decomposition to bromide and oxygen (rxn 12) was studied using a RuO_2 catalyst which was chosen based on previous reports.[40,41,42,43,44] The catalyst was synthesized using the Adams method[45] as described in the **Methods** section. The RuO_2 Adams catalyst was composed of the rutile phase as evidenced from the XRD diffractogram presented in **Extended Data Figure 4a**. It had a granular structure comprising sub-micron aggregates, as shown in SEM and TEM micrographs presented in **Extended Data Figure 4b-c**, with a BET surface area of 170±5 m^2/g (**Figure S4b**) and pore sizes in the range of 50-58 Å (**Figure S4c**). The conversion of bromate to bromide was measured by monitoring the volume of the effluent gas (oxygen) as a function of time during the catalytic decomposition of 1.5M $NaBrO_3$ aqueous solution (pre-heated to 60°C) in the presence of the catalyst, using the water displacement method (see **Methods** section for details, a picture of the system in **Extended Data Figure 5**, and **Video S5**). We note that some of the catalyst was washed away by the effluent gas out of the catalytic cell, as shown by the dark color of the tube connecting the cell to the water column. This artefact disables precise quantitative assessment of the specific activity of the catalyst. Nevertheless, the experiments presented herein suffice as a proof-of-concept to demonstrate the process functionality and performance. Future development of this process should immobilize the catalyst by embedding it in a porous support.

First, we examined the effect of borate and phosphate buffers (0.1M) on the reaction kinetics, using ~50 mg of the RuO_2 Adams catalyst. **Figure 4a** presents the degree of conversion of bromate to bromide as a function of time for the baseline solution (1.5M $NaBrO_3$) without (black curve) and with borate and phosphate buffers (blue and red curves, respectively). Without a buffer, full conversion is achieved in ~1.2 h, and the initial reaction rate is 0.0362 s^{-1}. Buffer addition (0.1M) to the baseline electrolyte has an adverse effect on the bromate decomposition kinetics (**Figure 4a**), which is worse for phosphate buffer than for borate buffer. For the borate buffer, the initial reaction rate is 0.0068 s^{-1} and full conversion is achieved in ~2.5 h, whereas for the phosphate buffer the initial reaction rate drops to 0.0041 s^{-1} and full conversion is not achieved in the timeframe of this measurement (10 h). Next, the effect of $Cr_2O_7^{2-}$ (3 mM) on the reaction kinetics was examined, using 25 mg of the RuO_2 Adams catalyst. The results are presented in **Figure 4b**. In the $NaBrO_3$ electrolyte without $Cr_2O_7^{2-}$ (black curve) full conversion is achieved in ~2.8 h and the initial reaction rate is 0.0349 s^{-1}. The addition of $Na_2Cr_2O_7$ reduces the initial reaction rate to 0.0168 s^{-1}, and delays the achievement of full conversion to ~6.4 h. The catalytic deactivation in the presence of phosphate and borate buffers and $Cr_2O_7^{2-}$ additive could possibly be attributed to the competitive adsorption of their ions on the surface of the catalyst which interferes with the bromate adsorption on the active centers. The extent of deactivation depends on the type and concentration of the interfering species, therefore tuning these parameters is important for the seamless operation of our process.

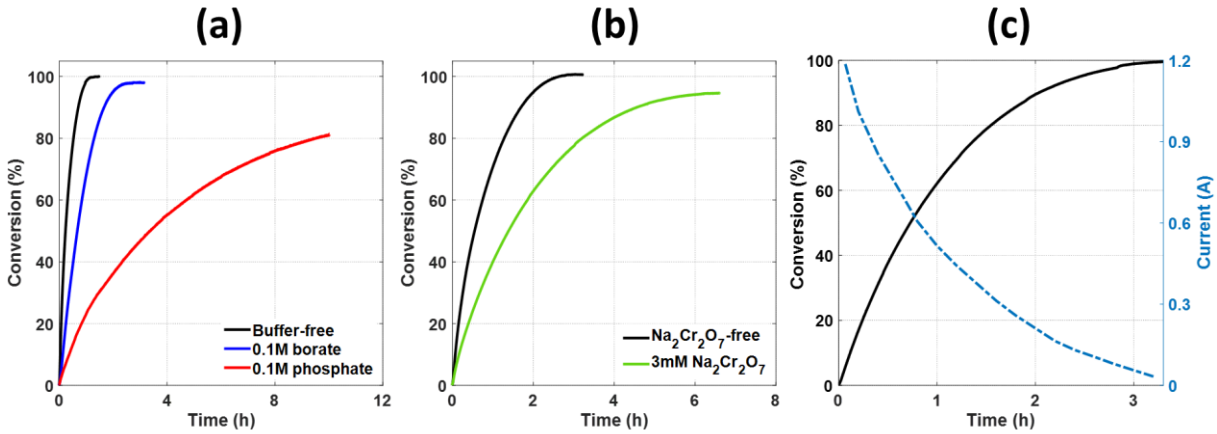

Figure 4. Catalytic decomposition of bromate to bromide and oxygen: Buffer effect **(a)** and $Na_2Cr_2O_7$ effect **(b)** on the catalytic conversion of BrO_3^- to Br^- and O_2 (rxn 12). The electrolyte was 1.5M $NaBrO_3$ (7 mL) and the catalyst mass was ~50 mg in **(a)** and **(c)**, and ~25 mg in **(b)**; **(c)** Catalytic conversion of 1M bromate solution obtained by bromide electrolysis (**Figure 2b**). The solid black curve presents the degree of conversion of bromate to bromide, and the dashed blue curve presents the equivalent electric current.

Batch-to-batch process: To demonstrate the feasibility of our process (**Figure 1**) we combined the electrolytic and catalytic sub-processes into a batch-to-batch process. An aliquot of 7 ml out of 20 ml of the oxidized electrolyte was taken from the best performance electrolytic test (**Figure 2b**) after converting 1M of bromide to bromate, and was transferred to the catalytic cell with 50 mg of the RuO_2 Adams catalyst that decomposed the bromate anions to bromide anions and oxygen. The volume of the effluent gas (oxygen) was measured (**Extended Data Figure 6**) and converted to degree of conversion, presented as a function of the reaction time in **Figure 4c** (black solid curve). The results show complete conversion (100%) of electrolytically obtained bromate to bromide and oxygen after ~3 h. This demonstrates a full cycle of hydrogen evolution and bromide electrooxidation to bromate with ~100% Faradaic efficiency in the electrolytic cell, coupled with complete conversion of the bromate formed in the electrolytic cell back to bromide with stoichiometric oxygen evolution in the catalytic cell.

Coupling the electrolytic and catalytic cells in a joint flow system is beyond the scope of this study, which presents a proof-of-principle of a new DWE process and demonstrates it basic functionality and performance. In a complete system with continuous electrolyte flow between the two cells it is important to match the rate of bromate formation in the electrolytic cell with the rate of its conversion back to bromide in the catalytic cell. To compare these rates in our system, the rate of oxygen evolution that was measured in the catalytic cell was converted to an equivalent electric current, I_{eq}, by assigning four electrons per O_2 molecule, shown by the dashed blue curve in **Figure 4c**. At the beginning of the reaction, the conversion rate corresponds to a high current of over 1 A. This indicates a fast catalytic reaction that would not limit the electrolytic reaction. In future development of the continuous process several parameters should be tuned to match the rates of the bromate formation and decomposition in the electrolytic and catalytic cells, respectively. In the electrolytic cell, the applied current density, electrode size, and the electrolyte composition and volume should be adjusted. In the catalytic cell, the length and diameter of the catalytic column, the amount of catalyst and the porous support in which it is embedded should be properly matched with the electrolytic current and electrolyte flow rate to support a seamless continuous operation.

Summary

This work presents a new decoupled water splitting process that produces hydrogen and oxygen in separate electrolytic and catalytic cells, respectively, and supports continuous operation in a membraneless system. We demonstrate high efficiency and high rate in a near-neutral electrolyte of NaBr in water, whereby bromide is oxidized to bromate concurrent with hydrogen evolution in the electrolytic cell, and bromate is reduced to bromide in a catalytic reaction that evolve oxygen in the catalytic cell. A Faradaic efficiency of 98±2% was achieved in a 1.5M NaBr electrolyte with 3.8 mM $Na_2Cr_2O_7$ that prevents cathodic loss reactions by coating the cathode, *in-situ* during operation, with a barrier layer that hinders the electroreduction of oxidized brome species. Under these conditions, no oxygen evolves in the electrolytic cell, enabling safe operation without dividing the cell into cathodic and anodic compartments using expensive membrane and sealing components as in conventional water electrolysis. Adding a borate buffer enhances the hydrogen evolution reaction and reduced the electrolytic cell voltage (IR-corrected) to 1.5 V at a current density of 5 mA/cm^2, or 2.4 V at 1 A/cm^2. These values correspond to electrolytic efficiency of 97.6%$_{HHV}$ and 61.7%$_{HHV}$ at low and high current densities, respectively, outperforming previous reports on decoupled water splitting using electron-coupled-proton buffers. [10-15,17] The electrolytic efficiency of our system is slightly lower than that reported in E-TAC water splitting,[8] but our process supports continuous operation without thermal swings, unlike E-TAC which is a batch process with thermal swings between cold (~25°C) and hot (~95°C) electrolytes that give rise to operational and heat management challenges. Another advantage of our process is operation in a near-neutral electrolyte, unlike previous reports on decoupled water splitting in acid or alkaline electrolytes. We also demonstrate fast reduction of the oxidized electrolyte taken from the electrolytic cell by a RuO_2 Adams catalyst in a simple catalytic cell, which is the key to integration of the electrolytic and catalytic sub-processes into a seamless process that splits water and produces hydrogen and oxygen continuously under constant electrolyte flow from one cell to another. Further efforts to develop this breakthrough process into a competitive technology for green hydrogen production should aim at the following goals: (1) Replacing the Pt cathode and RuO_2 anode (DSA) and catalyst (RuO_2 Adams) we used in our proof-of-concept experiments by Earth-abundant alternatives; (2) Replacing the $Na_2Cr_2O_7$ additive by non-toxic alternatives; (3) Integrating the electrolytic and catalytic sub-processes into a seamless process and validating its long-term performance.

Methods

Chemicals. Double distilled water (DDW, Direct-Q3 UV, Merck) was used to prepare the aqueous solutions. Piranha solution, comprising a 2:5 mixture of concentrated hydrogen peroxide H_2O_2 (30%, for analysis, Merck) and sulfuric acid H_2SO_4 (95-98%, AR, Bio-Lab, Israel), was used for cleaning the electrochemical cells, glassware, and Pt electrodes before use. Acetone (AR, Bio-Lab, Israel) and ethanol (absolute, AR, Gadot-Group, Israel) were used for cleaning the anode before use. The electrolytes were prepared using sodium bromide NaBr (99+%, Alfa Aesar). The pH values were adjusted with the use of sodium hydroxide NaOH (pearls, AR, Bio-Lab, Israel) solutions. The buffer solutions were prepared with the use of boric acid H_3BO_3 (99.6%, ACS grade, Acros), and phosphate dipotassium phosphate K_2HPO_4 (ACS grade, Spectrum chemical) and monopotassium phosphate KH_2PO_4 (ISO for analysis, Merck). Sodium dichromate dihydrate $Na_2Cr_2O_7 \times 2H_2O$ (ACS grade, Merck) was used as an additive in the electrolyte. Ar gas (Maxima, Israel, 99.999%) was used for purging the electrolyte in the polarization measurements. Ruthenium trichloride hydrate $RuCl_3 \times H_2O$ (35-40% Ru,

Acros Organics) and sodium nitrate $NaNO_3$ (99+%, ACS grade, Acros) were used for the synthesis of ruthenium dioxide powder (RuO_2 Adams catalyst). Potassium iodide KI (ACS reagent, Spectrum Chemical) and standardized 0.1N solution of sodium thiosulfate (Alfa Aesar) were used for iodometric titration of bromate solutions. Sodium bromate $NaBrO_3$ (99.5% metal basis, Alfa Aesar) was used to prepare the solutions for the water displacement measurements.

Electrodes. Pt foil (geometric area 0.2 cm^2, surface roughness factor ca. 3-4, 99.95%, 0.05 mm thick, Holland Moran, Israel) and Pt coil (wire diameter 5 mm, coil diameter and length are 4 and 15 mm, respectively, ALS Co., Japan) electrodes were used as cathodes in the bromide electrolysis measurements presented in **Figures 2b** and **2c**, respectively. The same Pt foil (2 cm^2) was used as the working electrode (WE) in the cathodic polarization HER measurements presented in **Figure 3b**. A smaller piece (0.45 cm^2) of the same Pt foil was used for the high current density measurements presented in **Figure 3a**, to comply with the maximum current limitation (800 mA) of the potentiostat (BioLogic SP-150). The Pt electrodes were cleaned by dipping into piranha solution and then thorough rinsing in DDW before measurements. Commercial RuO_2-TiO_2/Ti dimensionally stable anodes (DSA) (Ti substrate thickness 1 mm, thickness of mixed oxide layer ~20-30 µm (**Figure S2**), DSA10k, De Nora, Italy) were used as anodes, keeping the geometric area close to that of the corresponding cathode. The DSA anodes were pre-cleaned in a mixture of DDW/ethanol/acetone for 10 min in an ultrasound bath (MRC ultrasonic cleaner, 3L, 120W) and then thoroughly rinsed in DDW. A reversible hydrogen electrode (RHE) (HydroFlex, Gaskatel) was used as the reference electrode (RE) in the three-electrode measurements. It was immersed into the respective electrolyte 1 h before starting the measurements.

RuO_2 Adams catalyst synthesis. The RuO_2 Adams catalyst used in the bromate reduction process (**Figure 4**) was prepared, following a modified Adams process, [40,45] by grinding together 2 g of $RuCl_3$ xH_2O and 10 g of $NaNO_3$ powders with mortar and pestle. The resulting mixture was heated for 5 min in an oven (ELF Laboratory Chamber Furnace, max 1100°C, Carbolite) at 500°C. The oven was placed in a fume hood to safely remove toxic by-products of the reaction such as nitrogen oxide (NO/NO_2) gases. The resulting RuO_2 Adams catalyst was then cooled to ambient temperature and washed with DDW. The washing was repeated 3 times by means of centrifugation (MRC, SCEN-206 centrifuge) and decantation of the unreacted reagents in DDW. The recovered catalyst powder was then dried in air for several days.

Faradaic efficiency measurements. The Faradaic efficiency of bromide electro-oxidation to bromate (rxn 6) was evaluated for two operational modes under the experimental conditions described in **Extended Data Table 1**, using a RuO_2-TiO_2/Ti DSA anode and Pt foil/coil cathode in the same compartment (**Figure 2b** and **Figure 2d**, respectively). The amount of generated bromate anions was determined at the end of each of the electrolysis tests by iodometric titration and compared with the electric charge, $I \times t$ (I – current, t – electrolysis time), that passed between the electrodes during each test. In the first operational mode (**Figure 2a**), a double-jacketed electrochemical cell (Dr. Bob, Gamry, **Figure 2a**) was used, and the electrolyte, 1.5M NaBr without additives (experiments #1 and #3 in **Extended Data Table 1**) or with 3.8 mM $Na_2Cr_2O_7$ (experiment #2 in **Extended Data Table 1**), was heated to 60°C and stirred at 400 rpm using a Teflon coated magnetic stirrer. In the second operational mode (**Figure 2d**, experiments #4 and #5 in **Extended Data Table 1**), a cylindrical cell (graduated Pyrex cylinder, 20 ml, Duran) was used, and the electrolyte (1.5M NaBr, without additives) was kept at room temperature. The initial pH of the 1.5M NaBr electrolyte without additives was 5.8, whereas with the $Na_2Cr_2O_7$ additive it was 7.5.

Long-term stability. Extended Faradaic efficiency measurements were carried out during 5 consecutive days with 119 h of continuous electrolysis at a current of 300 mA (current density of 150 mA/cm^2). A large (500 ml) cylindrical cell with a Pt foil cathode and DSA anode was filled with 300 ml of the electrolyte (initial concentration: 1.5M NaBr, 0.3M borate buffer, and 3.8 mM $Na_2Cr_2O_7$), see photograph in **Extended Data Figure 1a**. The cell was heated to 60°C and stirred at 400 rpm. To reduce evaporation, the cap was sealed to the cell with Parafilm laboratory film. The bromide and bromate concentrations were measured by sampling the electrolyte approximately every 24 h during the test, and analyzing the sample composition by iodometric titration and ion chromatography. The results are presented in **Extended Data Figure 1b** and **1c**, respectively. The pH was measured each day and the resulted were in the range of 8.0 to 8.6.

Iodometric titration. Iodometric titration[46,47] was used to determine the concentration of bromate anions (BrO_3^-) in the electrolyte after bromide electrolysis tests. The bromate anions were reduced to bromide anions (Br^-) in the presence of excessive amount of iodide anions in acidic medium, $\mathrm{BrO_3^- + 6I^- + 3H_2SO_4 \rightarrow 3I_2 + Br^- + 3SO_4^{2-} + 3H_2O}$, and the liberated iodine (I_2) molecules were titrated by standardized thiosulfate solution, $\mathrm{2Na_2S_2O_3 + I_2 \rightarrow 2NaI + Na_2S_4O_6}$. To this end, a solution of 3.8 g of KI in 40 ml DDW was added to an aliquot of 400 µl (V_{aliquot}) that was collected from the electrolytic cell ($V_{\mathrm{electrolyte}} = 20\ \mathrm{ml}$) at the end of the electrolysis experiment, followed by addition 0.6 ml of concentrated sulfuric acid H_2SO_4. After dilution by DDW to a volume of 50 ml the resultant dark-violet solution (**Figure S4**, left) was gradually titrated by adding a standardized 0.1N solution of sodium thiosulfate $Na_2S_2O_3$ ($C_{S_2O_3^{2-}} = 0.1\mathrm{M}$) until reaching a transparent solution (**Video S3** and **Figure S4**, right). The volume of the thiosulfate solution that was added to this point, $V_{S_2O_3^{2-}}$, was used to calculate the amount of bromate ions that was generated by the electrolysis: $n_{BrO_3^-} = \frac{1}{6}\frac{V_{S_2O_3^{2-}}\ C_{S_2O_3^{2-}}}{V_{\mathrm{aliquot}}} V_{\mathrm{electrolyte}}$.

Ion chromatography. Ion chromatography was used to measure the concentration of bromide and bromate anions in the sampled solutions during the long-term stability measurement **(Extended Data Figure 1)**, using a Metrohm 881 Compact IC pro chromatograph equipped with a Shodex IC-SI-52 4E analytical column. Two 100 µl duplicate samples were collected approximately every 24 h since the beginning of the test and diluted by DDW to prepare 4 ml samples that were analyzed by ion chromatography using bromate and bromide standards from Sigma Aldrich.

Cathodic polarization measurements. The cathodic polarization curves presented in **Figure 3b** were measured by linear sweep voltammetry in a three-electrode water-jacketed electrochemical cell (Dr. Bob), using a Pt foil (2 cm^2) as working electrode (WE) and a potentiostat (BioLogic SP-150) at a scan rate 1 mV/s. A Pt wire (diameter 5 mm, Gamry) placed in a separate fritted glass compartment was used as a counter electrode (CE), where bromide electro-oxidation took place. A reversible hydrogen electrode (RHE) was used as a reference electrode (RE). The RE and WE were placed in the same compartment. The series resistance *R* was measured by current interruption method before each measurement. Measurements were carried out in Ar-purged 1.5M NaBr electrolytes containing different additives at 60°C. The basicity of the electrolyte was adjusted to pH 8 using a 5M NaOH solution using an Oakton pH/mV/°C pH-meter (series 500). In short experiments that correspond to several polarization curves, the addition of sodium dichromate to the electrolyte was found to have a negligible effect on the polarization curves, therefore it was not used in the cathodic polarization

measurements. No stirring was applied in these measurements to minimize interference by back reactions of the products of bromide electro-oxidation at the CE.

Anodic polarization measurements. The anodic polarization curves presented in **Figure 3c** were measured similarly to the cathodic polarization measurements, with the following exceptions: First, a DSA10K anode (2 cm^2) was used as a WE; and second, the WE and CE (Pt coil) were placed in the same compartment, so that the hydroxide anions (OH^-) formed at the CE (rxn 1) would not be restricted to react with Br_2 formed at the WE (rxn 2) in the bulk solution (rxn 3).

Electrolytic efficiency. The electrolytic efficiency of the hydrogen and bromate evolution reactions (HER and BER, respectively) were evaluated from the steady-state current - voltage curve presented in **Figure 3a**. To this end, galvanostatic measurements were carried out at different currents in a two-electrode cell configuration (**Figure 2a**) using a BioLogic SP-150 potentiostat with a Pt foil cathode and a DSA10K anode. The electrolyte was 1.5M NaBr with sodium dichromate additive (3.8 mM), without a buffer or with 0.7M borate buffer (black and blue curves in **Figure 3a**, respectively). The electrolyte was heated to 60°C in a double-jacketed electrochemical cell (Dr. Bob) and stirred at 400 rpm. Current density values from 5 to 1000 m/cm^2 were applied in ascending order, holding for 5 min at a time, while monitoring the applied voltage. The voltage values were averaged to obtain the mean value and standard deviation at each current density and corrected for the Ohmic (IR) drop. The resistance R was measured by electrochemical impedance spectroscopy (EIS) using a BioLogic SP-150 potentiostat and was determined as the high-frequency intercept with the real axis in the Nyquist plot. The EIS measurements were conducted in a galvanostatic mode at the same currents of the current – voltage measurements, with an oscillation amplitude of 5% of the mean current and oscillation frequency from 200 kHz to 100 mHz. The IR-corrected mean voltage values, V_{cell}, were used to calculate the electrolytic efficiency based on the higher heating value (HHV) of hydrogen, $\eta = (1.48/V_{cell})\times 100\%_{HHV}$.

Bromate catalytic decomposition. The water displacement technique[48,49,50] was used to monitor the kinetics of the bromate catalytic decomposition (rxn 12) on the RuO_2 Adams catalyst (**Figure 4**). The method is based on weighing the amount of water displaced by the oxygen released in the reaction. The experimental setup, presented in **Extended Data Figure 5**, comprises of a gas-tight glass reactor placed in a water bath on top of a heated plate and a water column. The outlet of the reactor is connected to the inlet of a water column, whereas the outlet of the column is directed to a beaker that is placed on a digital balance that monitors the mass change as a function of time during the decomposition reaction. Before the start of the experiment, the tube is closed by a metal pinch clamp. To start the measurement, a known volume (V_{sol} = 7 ml) of $NaBrO_3$ solution with a known concentration of bromate anions ($C_{BrO_3^-}$ = 1.5M) is added to the reactor that contains a known mass of the RuO_2 Adams catalyst (m_{RuO_2}). Then, the reactor is sealed, and the pinch clamp is opened. The oxygen gas that evolves in the reactor flows to the water column through the tube and displaces the water from the column to the beaker, and the mass of the displaced water (m_{water}) is constantly measured (**Video S5**). The measured mass (in kg) is nearly equal to oxygen volume (V_{O_2}, in L) since the density of water is 0.998 kg/L in STP. The oxygen volume, V_{O_2}, is converted to number of moles of oxygen, n_{O_2}, by the ideal gas law ($PV = nRT$). Taking a ratio of 2:3 between the bromate anions converted to bromide and the generated O_2 molecules (rxn 12), the degree of conversions is $2\, n_{O_2} / 3\, V_{sol}\, C_{BrO_3^-}$, presented in **Figure 4** as a function of the reaction time (t). The slope $s = dn_{O2}/dt$ yields a

reaction rate, which can be converted to an equivalent electric current $I = 4 \times F \times s$ (presented in **Figure 4c**, blue curve), where F is Faraday's constant and 4 in the number of electrons needed to generate an oxygen molecule by the oxygen evolution reaction. The conversion degree values were verified independently by end-of-experiment iodometric titrations, confirming full decomposition of bromate to bromide with close to 100% oxygen yield at the end of the experiments.

The water displacement technique was applied for a series of experiments with different catalyst to solution volume ratios and with different electrolyte additives including dichromate, phosphate buffer and borate buffer (**Extended Data Table 3**).

Acknowledgement

This research was supported by the Ministry of Innovation, Science and Technology, Israel (grant no. 1001577992), and by the KKL-JNF Climate and KKL-JNF Climate Solution Prize. A.R. acknowledges the support of the L. Shirley Tark Chair in Science.

References:

1. Krishnan, S. *et al.* Present and future cost of alkaline and PEM electrolyser stacks. *Int. J. Hydrogen Energy* (2023) doi:10.1016/j.ijhydene.2023.05.031.
2. Howarth, R. W. & Jacobson, M. Z. How green is blue hydrogen? *Energy Sci. Eng.* **9**, 1676–1687 (2021).
3. McHugh, P. J., Stergiou, A. D. & Symes, M. D. Decoupled Electrochemical Water Splitting: From Fundamentals to Applications. *Adv. Energy Mater.* **10**, 2002453 (2020).
4. Ifkovits, Z. P., Evans, J. M., Meier, M. C., Papadantonakis, K. M. & Lewis, N. S. Decoupled electrochemical water-splitting systems: A review and perspective. *Energy Environ. Sci.* **14**, 4740–4759 (2021).
5. Landman, A., Rothschild, A. & Grader, G. S. *New electrolyzer principles: decoupled water splitting*. *Electrochemical Power Sources: Fundamentals, Systems, and Applications Hydrogen Production by Water Electrolysis* (Elsevier B.V., 2021). doi:10.1016/B978-0-12-819424-9.00012-4.
6. Chen, L., Dong, X., Wang, Y. & Xia, Y. Separating hydrogen and oxygen evolution in alkaline water electrolysis using nickel hydroxide. *Nat. Commun.* **7**, 11741 (2016).
7. Landman, A. *et al.* Photoelectrochemical water splitting in separate oxygen and hydrogen cells. *Nat. Mater.* **16**, 646–651 (2017).
8. Dotan, H. *et al.* Decoupled hydrogen and oxygen evolution by a two-step electrochemical–chemical cycle for efficient overall water splitting. *Nat. Energy* **4**, 786–795 (2019).
9. Wang, J. *et al.* Decoupling half-reactions of electrolytic water splitting by integrating a polyaniline electrode. *J. Mater. Chem. A* **7**, 13149–13153 (2019).
10. Symes, M. D. & Cronin, L. Decoupling hydrogen and oxygen evolution during electrolytic water splitting using an electron-coupled-proton buffer. *Nat. Chem.* **5**, 403–409 (2013).
11. Rausch, B., Symes, M. D. & Cronin, L. A bio-inspired, small molecule electron-coupled-proton buffer for decoupling the half-reactions of electrolytic water splitting. *J. Am. Chem. Soc.* **135**, 13656–13659 (2013).
12. Kirkaldy, N., Chisholm, G., Chen, J. J. & Cronin, L. A practical, organic-mediated, hybrid

electrolyser that decouples hydrogen production at high current densities. *Chem. Sci.* **9**, 1621–1626 (2018).

13. Chisholm, G., Cronin, L. & Symes, M. D. Decoupled electrolysis using a silicotungstic acid electron-coupled-proton buffer in a proton exchange membrane cell. *Electrochim. Acta* **331**, 135255 (2020).

14. Li, W. *et al.* Electrolyzer Design for Flexible Decoupled Water Splitting and Organic Upgrading with Electron Reservoirs. *Chem* **4**, 637–649 (2018).

15. Zhang, F. *et al.* Decoupled Redox Catalytic Hydrogen Production with a Robust Electrolyte-Borne Electron and Proton Carrier. *J. Am. Chem. Soc.* **143**, 223–231 (2021).

16. Landman, A. *et al.* Decoupled Photoelectrochemical Water Splitting System for Centralized Hydrogen Production. *Joule* **4**, 448–471 (2020).

17. Rausch, B., Symes, M. D., Chisholm, G. & Cronin, L. Decoupled catalytic hydrogen evolution from a molecular metal oxide redox mediator in water splitting. *Science* **345**, 1326–1330 (2014).

18. Amstutz, V. *et al.* Renewable hydrogen generation from a dual-circuit redox flow battery. *Energy Environ. Sci.* **7**, 2350–2358 (2014).

19. Symes, M. D. Just add hot water. *Nat. Energy 2019 49* **4**, 730–731 (2019).

20. Centi, G. Across the Board: Gabriele Centi on Decoupling Electrocatalytic Reactions to Electrify Chemical Production. *ChemSusChem* **15**, e202200007 (2022).

21. Park, S.-H. *et al.* Quantifying the Trade-Off between Absolute Capacity and Rate Performance in Battery Electrodes. *Adv. Energy Mater.* **9**, 1901359 (2019).

22. Bazant, M. Z. Theory of chemical kinetics and charge transfer based on nonequilibrium thermodynamics. *Acc. Chem. Res.* **46**, 1144–1160 (2013).

23. Suen, N. T. *et al.* Electrocatalysis for the oxygen evolution reaction: recent development and future perspectives. *Chem. Soc. Rev.* **46**, 337–365 (2017).

24. Bratsch, S. G. Standard Electrode Potentials and Temperature Coefficients in Water at 298.15 K. *J. Phys. Chem. Ref. Data* **18**, 1–21 (1989).

25. CRC Handbook of Chemistry and Physics. *CRC Handb. Chem. Phys.* (2016) doi:10.1201/9781315380476.

26. Grinbaum, B. & Freiberg, M. Bromine. *Kirk-Othmer Encycl. Chem. Technol.* (2002) doi:10.1002/0471238961.0218151310010311.A01.PUB2.

27. Amoore, J. E. & Hautala, E. Odor as an ald to chemical safety: Odor thresholds compared with threshold limit values and volatilities for 214 industrial chemicals in air and water dilution. *J. Appl. Toxicol.* **3**, 272–290 (1983).

28. Viswanathan, K. & Tilak, B. V. Chemical, Electrochemical, and Technological Aspects of Sodium Chlorate Manufacture. *J. Electrochem. Soc.* **131**, 1551–1559 (1984).

29. Osuga, T. & Sugino, K. Electrolytic Production of Bromates. *J. Electrochem. Soc.* **104**, 448 (1957).

30. Cettou, P., Robertson, P. M. & Ibl, N. On the electrolysis of aqueous bromide solutions to bromate. *Electrochim. Acta* **29**, 875–885 (1984).

31. Pavlović, O. Ž., Krstajić, N. V. & Spasojević, M. D. Formation of bromates at a RuO2TiO2 titanium

anode. *Surf. Coatings Technol.* **34**, 177–183 (1988).

32. Vasudevan, S. Studies relating to electrolytic preparation of potassium bromate. *Ind. Eng. Chem. Res.* **47**, 1743–1746 (2008).

33. Gomes, A. S. O., Busch, M., Wildlock, M., Simic, N. & Ahlberg, E. Understanding Selectivity in the Chlorate Process: A Step towards Efficient Hydrogen Production. *ChemistrySelect* **3**, 6683–6690 (2018).

34. Endrődi, B., Sandin, S., Wildlock, M., Simic, N. & Cornell, A. Suppressed oxygen evolution during chlorate formation from hypochlorite in the presence of chromium(VI). *J. Chem. Technol. Biotechnol.* **94**, 1520–1527 (2019).

35. Endrődi, B., Simic, N., Wildlock, M. & Cornell, A. A review of chromium(VI) use in chlorate electrolysis: Functions, challenges and suggested alternatives. *Electrochim. Acta* **234**, 108–122 (2017).

36. Endrődi, B. *et al.* Towards sustainable chlorate production: The effect of permanganate addition on current efficiency. *J. Clean. Prod.* **182**, 529–537 (2018).

37. Amit, L., Naar, D., Gloukhovski, R., la O', G. J. & Suss, M. E. A Single-Flow Battery with Multiphase Flow. *ChemSusChem* **14**, 1068–1073 (2021).

38. Jackson, M. N., Jung, O., Lamotte, H. C. & Surendranath, Y. Donor-Dependent Promotion of Interfacial Proton-Coupled Electron Transfer in Aqueous Electrocatalysis. *ACS Catal.* **9**, 3737–3743 (2019).

39. Strmcnik, D. *et al.* Improving the hydrogen oxidation reaction rate by promotion of hydroxyl adsorption. *Nat. Chem.* **5**, 300–306 (2013).

40. Mills, A. & Meadows, G. Heterogeneous redox catalysis: A novel route for removing bromate ions from water. *Water Res.* **29**, 2181–2185 (1995).

41. Duonghong, D., Erbs, W., Shuben, L. & Grätzel, M. Efficient redox catalysis by RuO2 in the generation of oxygen and bromine from aqueous bromate solutions. *Chem. Phys. Lett.* **95**, 266–268 (1983).

42. Dong, Z., Dong, W., Sun, F., Zhu, R. & Ouyang, F. Effects of preparation conditions on catalytic activity of Ru/AC catalyst to reduce bromate ion in water. *React. Kinet. Mech. Catal.* **107**, 231–244 (2012).

43. Thakur, D. B. *et al.* Ruthenium catalyst on carbon nanofiber support layers for use in silicon-based structured microreactors. Part II: Catalytic reduction of bromate contaminants in aqueous phase. *Appl. Catal. B Environ.* **102**, 243–250 (2011).

44. Fan, C. *et al.* Enhanced performance and mechanism of bromate removal in aqueous solution by ruthenium oxide modified biochar (RuO2/BC). *Colloids Surfaces A Physicochem. Eng. Asp.* **572**, 27–36 (2019).

45. Adams, R., Voorhees, V. & Shriner, R. L. Platinum Catalyst for Reductions: Platinic oxide. *Org. Synth.* **8**, 92–92 (2003).

46. Vogel, A., Jeffery, G H., Bassett, J., Mendham, J., Denney, R. C. Vogel's Textbook of Quantitative Chemical Analysis Fifth Edition. *Longman Sci. Tech.* **5**, 406 (1989).

47. Asakai, T. & Hioki, A. Potassium bromate assay by primary methods through iodine liberation reaction. *Anal. Methods* **5**, 6240–6245 (2013).

48. Walker, M., Zhang, Y., Heaven, S. & Banks, C. Potential errors in the quantitative evaluation of biogas production in anaerobic digestion processes. *Bioresour. Technol.* **100**, 6339–6346 (2009).

49. El Asri, O., Mahaouch, M. & Afilal, M. E. The evaluation and the development of three devices for measurement of biogas production. *Phys. Chem. News* vol. 75 (2015).

50. Brack, P., Dann, S., Upul Wijayantha, K. G., Adcock, P. & Foster, S. A simple, low-cost, and robust system to measure the volume of hydrogen evolved by chemical reactions with aqueous solutions. *J. Vis. Exp.* **2016**, 54383 (2016).

Extended Data

Extended Data Table 1: Experimental conditions for Faradaic efficiency (FE) measurements. Electrolysis current 600 mA, electrolysis duration 5.36 h, 20 ml of 1.5M NaBr electrolyte (without buffer).

Experiment #	**Figure**	FE (%)	$Na_2Cr_2O_7$	Cell type	Cathode	Cathode coating	Temp. (°C)	Stirring (rpm)	pH initial	pH final
1		10±1	-	Double jacketed cell	Pt foil	-	60	400	5.8	9.2
2	**2a, b**	98±2	3.8 mM			In-situ*			7.5	7.9
3		80±2	-			Ex-situ#			5.8	9.5
4	**2c, d, e**	72±2	-	Cylindrical cell	Pt coil	-	RT	-	5.8	8.3
5		13±1	-					400	5.8	10.5

* In-situ coating by electrochemical reduction of $Cr_2O_7^{2-}$ anions during electrolysis.

Using precoated electrodes from prior electrolysis tests.

Extended Data Table 2. Experimental conditions for electrolytic efficiency experiments. All the measurements were carried out in a heated electrolyte (60°C). The initial pH was 8.

Figure	Method	Electrodes	Electrolyte	Buffer	Stirring
3a	Galvanostatic 2-electrode-cell	DSA anode Pt foil cathode	1.5M NaBr 3.8mM $Na_2Cr_2O_7$	-	400 rpm
				0.7M borate	
3b	LSV 3-electrode-cell	Pt foil WE Pt wire CE RHE RE	1.5M NaBr	-	-
				0.1M borate	
				0.4M borate	
				0.7M borate	
3c	LSV 3-electrode-cell	DSA WE Pt coil CE RHE RE	1.5M NaBr	0.1M borate	-
				0.4M borate	
				0.7M borate	

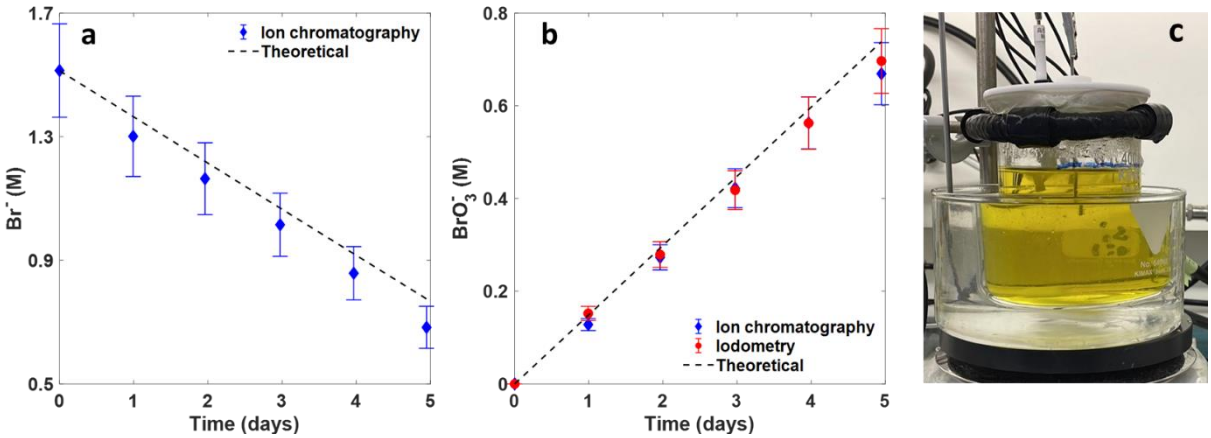

Extended Data Figure 1. Long term electrolysis stability. The bromide **(a)** and bromate **(b)** concentration during five days of continuous electrolysis of 300 ml aqueous solution of 1.5M NaBr (initial composition) with 0.3M borate buffer and 3.8 mM $Na_2Cr_2O_7$, at a current of 300 mA, temperature of 60°C, and stirring rate of 400 rpm. The data points and error bars present the mean values and standard deviation of two duplicates, measured by ion chromatography (blue) and iodometric titration (red). A photograph of the measurement setup in shown in **(c)**.

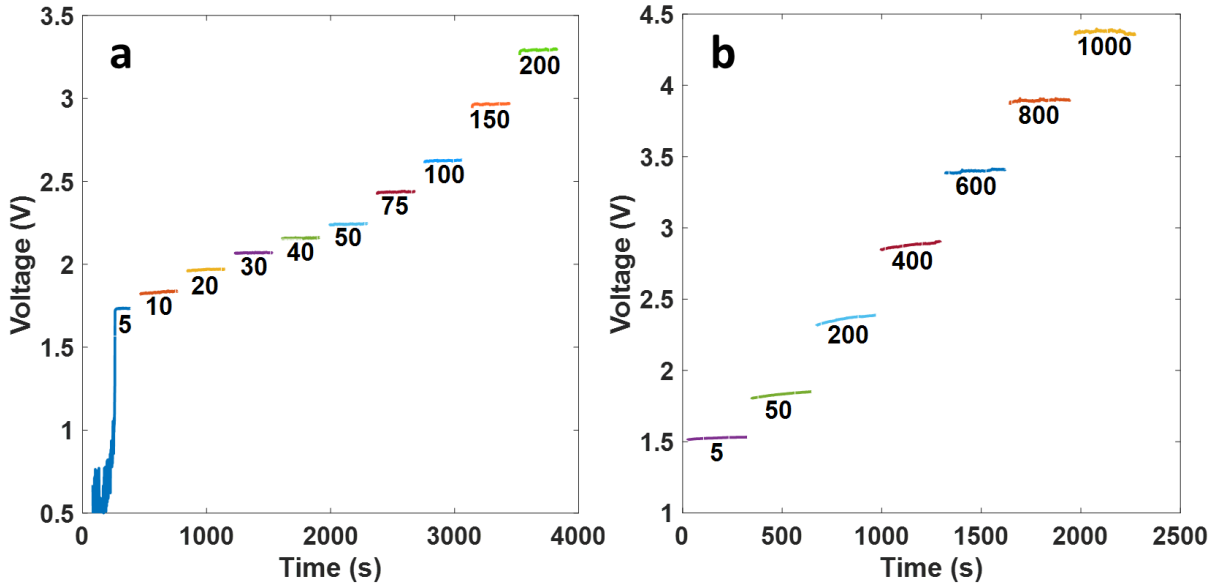

Extended Data Figure 2. Chronopotentiometry measurements at different current densities as indicated by the labels in the figures (in units of mA/cm^2)**. (a)** 1.5M NaBr, no buffer, 3.8 mM $Na_2Cr_2O_7$, 60°C, 400 rpm; **(b)** 1.5M NaBr, 0.7M borate buffer, 3.8 mM $Na_2Cr_2O_7$, 60°C, 400 rpm. The voltage is presented without IR correction.

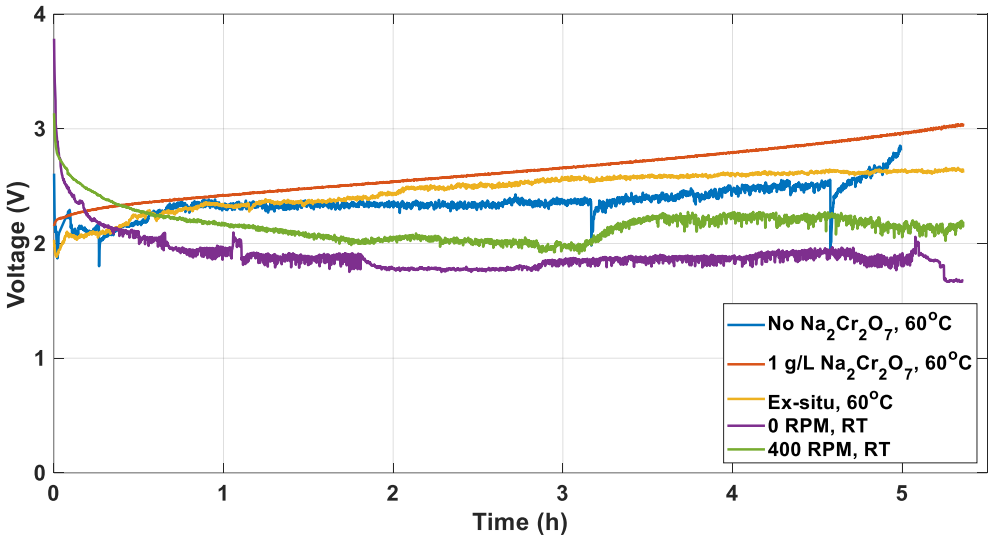

Extended Data Figure 3. **Long term stability of bromide electrolysis.** The voltage (IR corrected) as a function of time during extended galvanostatic measurements at a current of 600 mA in 1.5M NaBr electrolyte with (red curve) or without 3.8 mM $Na_2Cr_2O_7$ (all other curves) measured at 60°C (blue, red and orange curves) or at room temperature (purple and green curves) with (all curves expect for the purple curve) or without stirring (purple curve). Pristine Pt foil/coil (at 60°C/RT respectively) cathode and RuO_2/TiO_2 DSA anode were used in the measurements, except for the one presented by the orange curve where a pre-coated Pt foil cathode from previous electrolysis tests was used. The voltage drift in the red curve results from changes in the electrolyte composition due to conversion of bromide to bromate during the measurement.

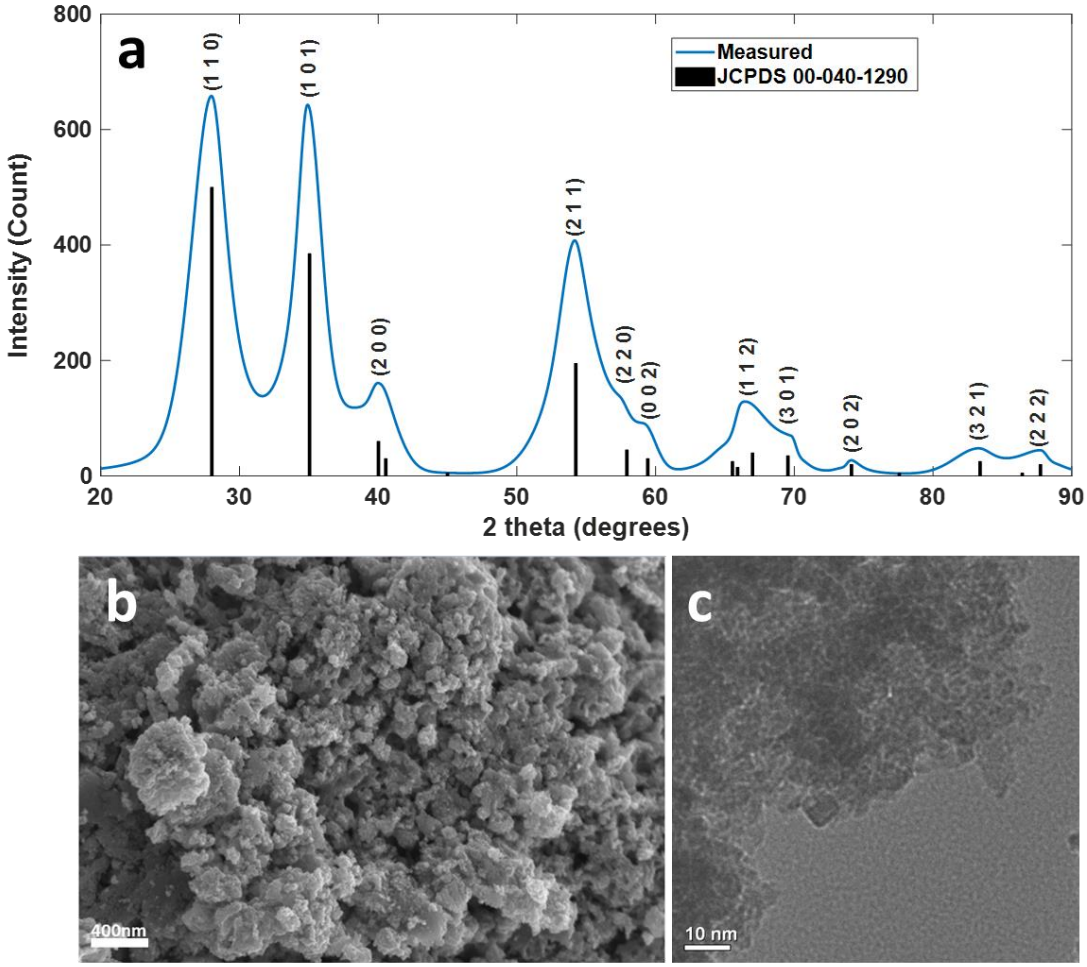

Extended Data Figure 4. **Ru Adams catalyst characterization. (a)** XRD pattern compared to the JCPDS data of tetragonal RuO_2; **(b)** SEM micrograph; **(c)** TEM micrograph.

Extended Data Table 3. Experimental conditions for catalytic decomposition experiments. All the measurements were carried out in a heated and stirred 1.5M $NaBrO_3$ electrolyte (60°C, 400 rpm). The initial pH was 8.

Figure	Initial rate (s^{-1})	RuO_2 Adams mass (mg)	Additives
-	0.0310	102.8	No
4a	0.0362	51.2	
4b	0.0349	25.5	
4a	0.0041	51.6	0.1M phosphate buffer
4a	0.0068	55.0	0.1M borate buffer
4b	0.0168	25.4	3 mM $Cr_2O_7^{2-}$

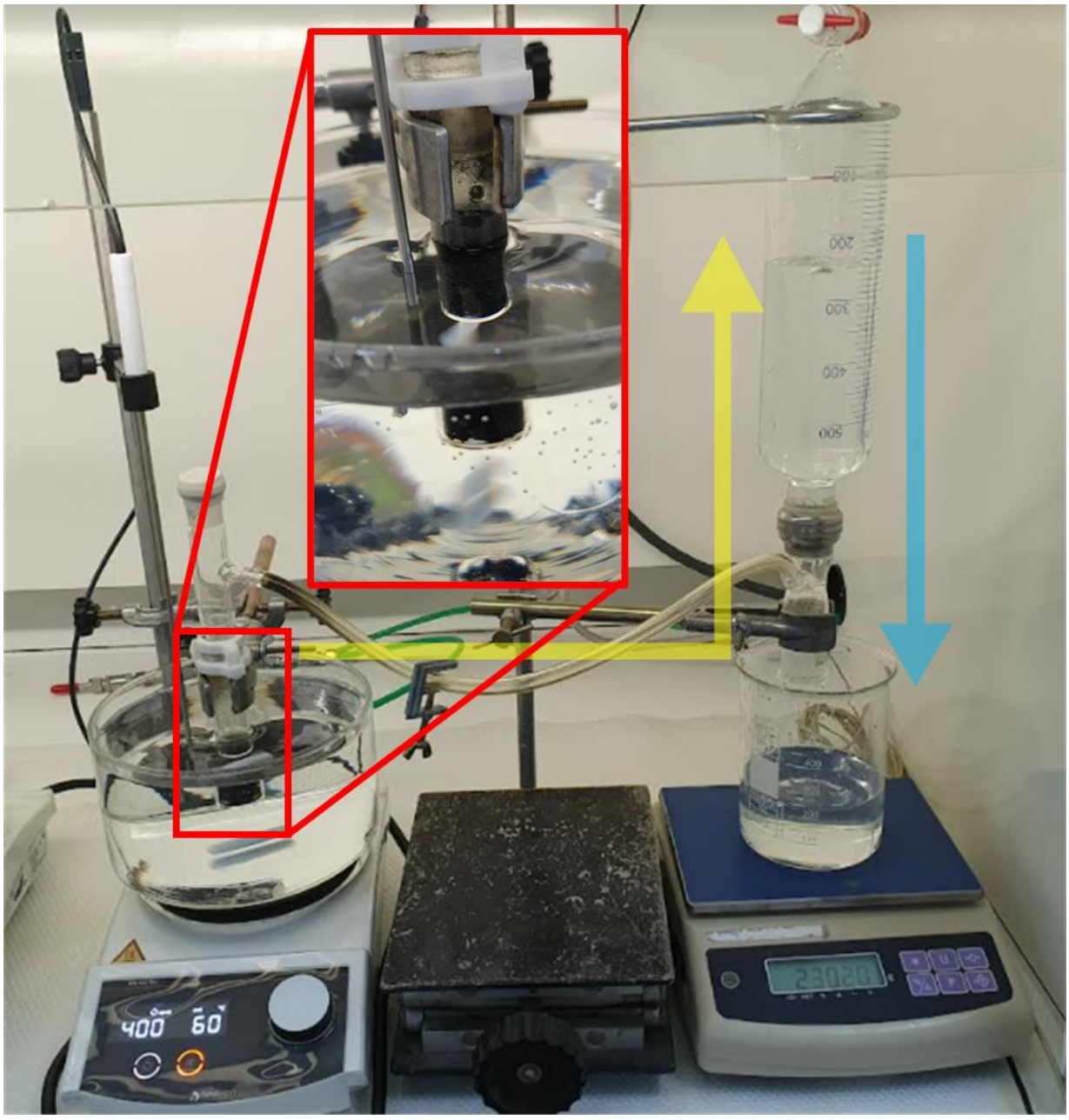

Extended Data Figure 5. Water displacement experimental setup.

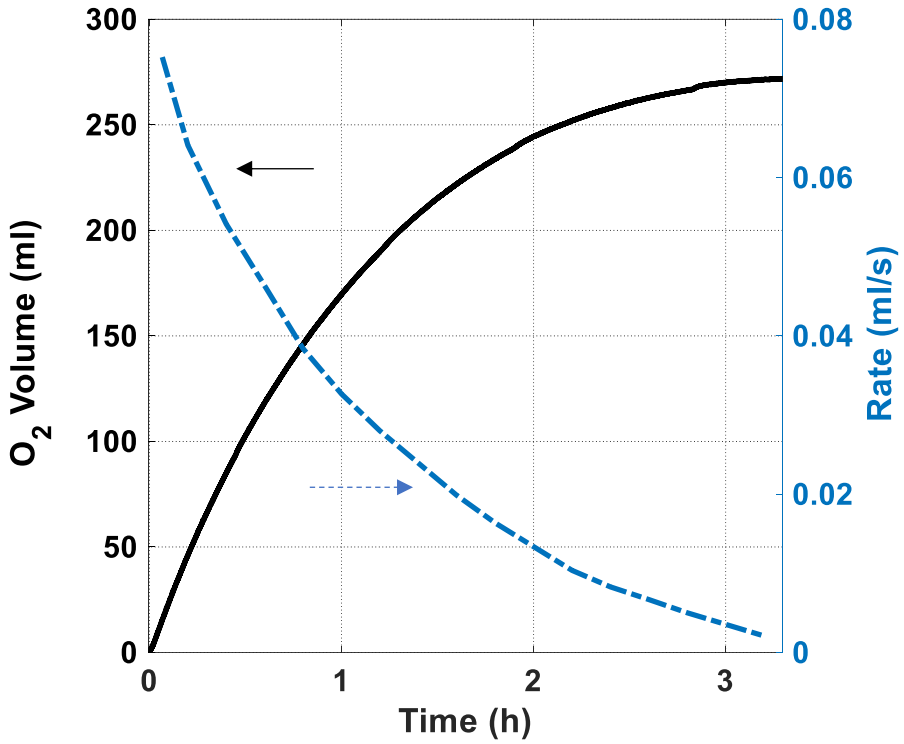

Extended Data Figure 6. **Catalytic conversion of 1M bromate solution obtained by bromide electrolysis** (**Figure 2b**). The solid black curve presents the evolved volume of oxygen due to bromate decomposition, and the dashed blue curve presents the oxygen evolution rate.